JACS
JOURNAL OF THE AMERICAN CHEMICAL SOCIETY
pubs.acs.org/JACS
Article

Three-State Switching of an Anthracene Extended Bis-thiaxanthylidene with a Highly Stable Diradical State

Marco B. S. Wonink, Brian P. Corbet, Artem A. Kulago, Gregory B. Boursalian, Bas de Bruin, Edwin Otten, Wesley R. Browne, and Ben L. Feringa*

Cite This: J. Am. Chem. Soc. 2021, 143, 18020–18028
Read Online
ACCESS | Metrics & More | Article Recommendations | Supporting Information

ABSTRACT: A multistable molecular switching system based on an anthracene-extended bis-thiaxanthylidene with three individually addressable states that can be interconverted by electrochemical, thermal, and photochemical reactions is reported. Besides reversible switching between an open-shell diradical- and a closed-shell electronic configuration, our findings include a third dicationic state and control by multiple actuators. This dicationic state with an orthogonal conformation can be switched electrochemically with the neutral open-shell triplet state with orthogonal conformation, which was characterized by EPR. The remarkably stable diradical shows kinetic stability as a result of a significant activation barrier for isomerization to a more stable neutral closed-shell folded geometry. We ascribe this activation barrier of $\Delta G^{\ddagger}$(293 K) = 25.7 kcal mol^{-1} to steric hindrance in the fjord region of the overcrowded alkene structure. The folded closed-shell state can be converted back to the diradical state by irradiation with 385 nm. The folded state can also be oxidized to the dicationic state. These types of molecules with multiple switchable states and in particular stable diradicals show great potential in the design of new functional materials such as memory devices, logic gates, and OFETs.

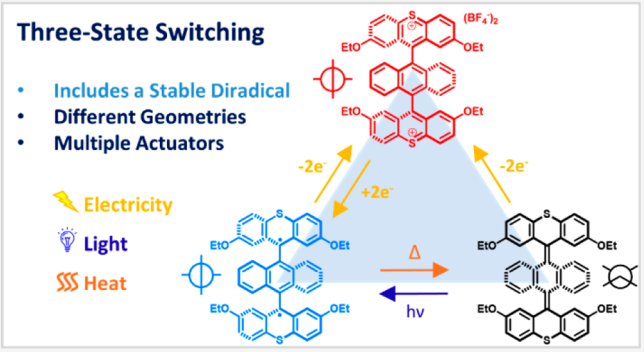

INTRODUCTION

Artificial molecular switches and motors play a prominent role in the transition from molecules with static function to dynamic molecular systems in contemporary chemistry.[1−3] Taking inspiration from biology, e.g., the process of vision, it is evident that molecular switching offers numerous opportunities for the reversible control of material properties,[4] molecular information content,[5] or biological function.[6] Switching between redox and geometric states can be induced by external stimuli including electricity, light, and heat.[7,8] A molecular switch can typically form either of two stable isomers, so-called bistability, to control, for example, magnetic, electronic, and optical properties, supramolecular assembly, and molecular recognition or complex functions such as catalysis.[9−15]

Moving beyond bistability, the design of multiple switchable molecular systems that can reach various stable states triggered by distinct and orthogonal external inputs e.g., photochemical, thermal, and electrochemical, remains particularly challenging. Herein, we report reversible switching between *three states in a single molecule*, including a highly stable diradical state, controlled through multiple actuators (electricity, light, and heat). Stable organic diradicals feature unique electronic properties and therefore show great potential for applications in molecular electronics such as organic field-effect transistors (OFETs).[16] Reversible switching between open-shell diradical (or diradicaloid) and closed-shell electronic configurations of organic molecules is fascinating both experimentally and theoretically.[17−20] The system we describe here adds a third state that is interconvertible with the open-shell diradical state via redox chemistry. We anticipate that such a system with three independently addressable states will open doors toward smart, tunable electronics such as memory devices and logic gates.[21]

The systems presented here are based on bistricyclic aromatic enes (BAEs),[22] a class of molecules that includes the overcrowded alkene light-driven molecular motors, which are robust examples of multistage switchable molecular systems.[23] In BAEs, the steric crowding in the fjord region plays a key role in the relative stability of various isomers.[22] Two such geometries are described as folded (**F**) and twisted (**T**) (Figure 1). Facing the challenge to design orthogonal switching systems to allow ultimately more complex dynamic

Received: June 8, 2021
Published: October 25, 2021

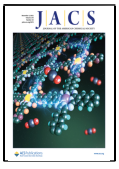

https://doi.org/10.1021/jacs.1c05938
J. Am. Chem. Soc. 2021, 143, 18020−18028

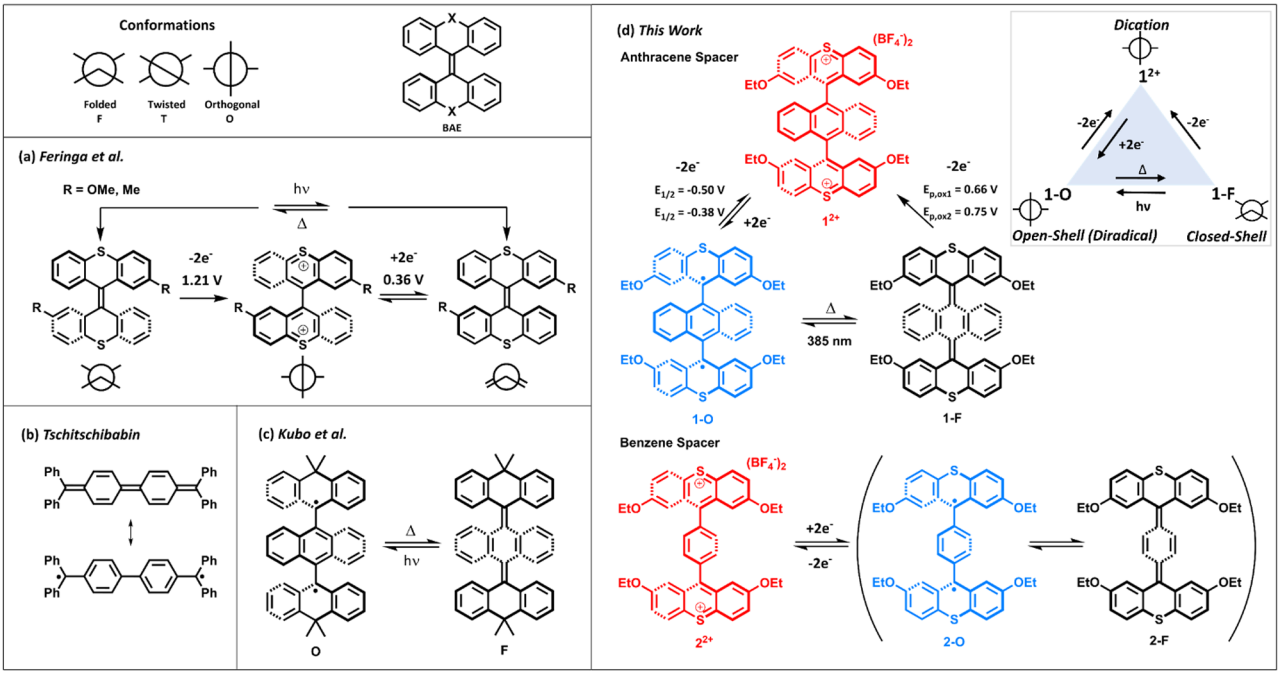

Figure 1. (a) Reversible switching of bis-thiaxanthylidenes from our earlier studies,[12] (b) Tschitschibabins's hydrocarbon,[24] (c) DMA-based switch from Kubo et al.,[18] and (d) our current work on aromatically extended bis-thiaxanthylidene switches.

and responsive behavior, bisthiaxanthylidenes, a specific class of BAEs, offer the opportunity to combine multiple effectuators and states.[12] Bisthiaxanthylidenes undergo geometrical changes induced by either redox or photochemical reactions. A photochemical-redox luminescent switch based on bisthiaxanthylidenes was developed earlier by our group, in which oxidation leads to a stable dicationic state with a nearly orthogonal (**O**) orientation of the two tricyclic aromatic moieties (Figure 1a).[12]

Recently, photochemical and thermal interconversion of stable closed-shell and open-shell diradical states of an organic compound (with a concomitant geometry change) has emerged as a new modality of molecular switching.[18] Organic compounds with an open-shell diradical resonance contributor in the ground state date back to Tschitschibabin's hydrocarbon, reported in 1907 (Figure 1b).[24,25] Noting the importance of stable open-shell systems, other organic compounds with diradicaloid ground states have since been described.[26−29] Bistability between open- and closed-shell states can be achieved when the activation barriers are sufficiently high,[18] while low barriers (with respect to k_BT) lead to thermal equilibration over the states.[30,31] The open-shell diradical configurations are stabilized by a combination of factors including steric hindrance, delocalization of spin density, and aromaticity.[32,33] In 2020, Kubo reported an organic compound capable of controlled switching between open-shell diradical and closed shell state: this BAE, based on the 9,10-dihydro-10,10-dimethyl-9-anthryl (DMA) motif, undergoes conversion from a triplet open-shell diradical state to a neutral closed-shell thermally, which can then be converted back to the open-shell state photochemically (Figure 1c).[18]

The anthracene-extended bis-thiaxanthylidene **1** described here allows for three-state reversible switching (Figure 1d). In our design the peripheral thioxanthene motif enables redox switching by stabilizing a dicationic state ($\mathbf{1}^{2+}$) by virtue of the sulfur heteroatom, which enables full conjugation to an "anthracene-like" delocalized structure facilitated by mesomeric electron donation (an effect that is entirely lacking in the DMA motif).[12,34] The thioxanthenes also stabilize an open-shell diradical configuration (**1-O**) in the neutral form by spin density delocalization.[35,36] Steric crowding in the fjord region caused by the central anthracene linker induces additional kinetic stabilization to the diradical. The stable open-shell orthogonal diradical converts thermally to a lower energy closed-shell folded geometry (**1-F**), and irradiation restores the compound to its orthogonal diradical state. In contrast, the analogous benzene-bridged bis-thiaxanthylidene **2** (Figure 1d) displays a thermal equilibrium between an open-shell diradical state (**2-O**) and a lower energy closed-shell folded state (**2-F**), which demonstrates the effect of steric crowding in the fjord region.

RESULTS AND DISCUSSION

Synthetic Procedures. The arene-extended bisthioxanthylium salts $\mathbf{1}^{2+}$ and $\mathbf{2}^{2+}$ were prepared with anthracene and benzene spacers, respectively (Scheme 1). Thioxanthen-9-one **3** was iodinated to obtain **4**, which was then functionalized with ethoxy groups through an Ullmann coupling to increase the solubility of these compounds in organic solvents. Dilithiation of 9,10-dibromoanthracene and 1,6-dibromobenzene and subsequent reaction with **5** produced diols **7** and **9**, respectively, which after dehydration with aqueous HBF_4 yielded the dicationic BF_4^- salts $\mathbf{1}^{2+}$ and $\mathbf{2}^{2+}$. Characterization of compound $\mathbf{1}^{2+}$ by ^{1}H NMR spectroscopy was precluded by the presence of traces of paramagnetic species, which is probably a monoradical impurity that facilitates fast electron exchange on the NMR time scale and consequent line broadening. The presence of a monoradical impurity is supported by an EPR signal that is typical for a doublet species (Figure S8). The salts $\mathbf{1}^{2+}$ and $\mathbf{2}^{2+}$ were reduced chemically with cobaltocene to obtain the neutral compounds

https://doi.org/10.1021/jacs.1c05938
J. Am. Chem. Soc. 2021, 143, 18020−18028

Scheme 1. Synthesis of Compounds 1^{2+}, 2^{2+}, 1-O, and 2-F

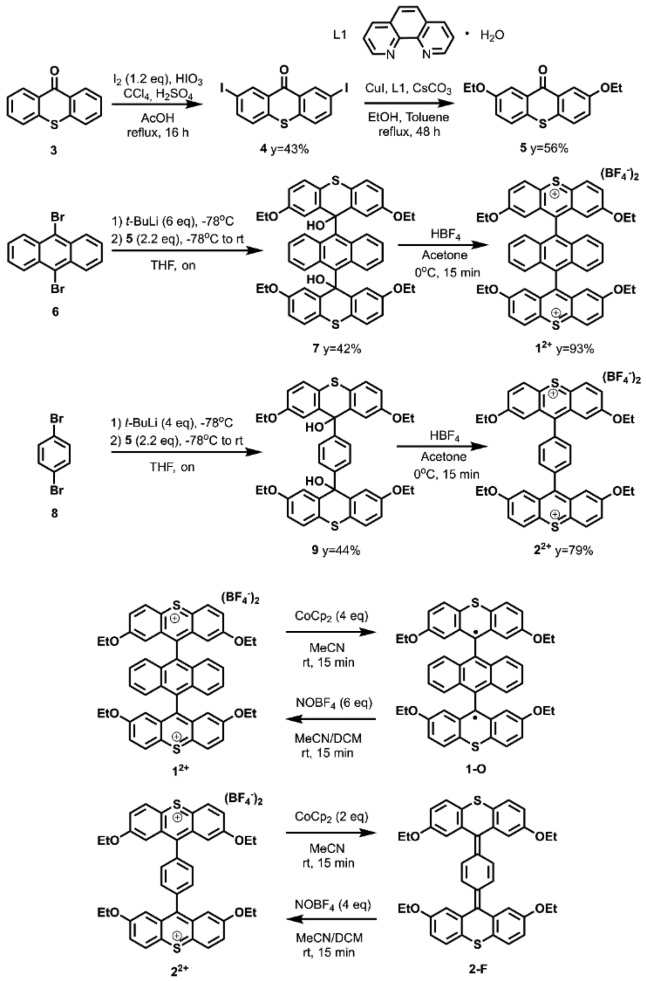

1-O and **2-F**. The ^{1}H NMR spectrum of compound **1-O** (Figure S2) shows paramagnetic shifts and broadening, consistent with open-shell diradical character. This is not the case for compound **2-F**, which we therefore expect to be in the lowest energy folded closed-shell state (DFT calculations *vide infra*), and we denote it as **2-F**. Reoxidation of **1-O** and **2-F** to their respective dicationic salts 1^{2+} and 2^{2+} was achieved with $NOBF_4$ (Figures S2 and S3).

X-ray Crystallography. Single-crystal X-ray analysis of 1^{2+} and **2-F** revealed the structures shown in Figure 2. DFT-optimized structures of **1-O** and 2^{2+} are shown in Figure 3. Both the anthracene-bridged dication 1^{2+} (Figure 2a) and the benzene-bridged dication 2^{2+} (DFT-optimized structure,

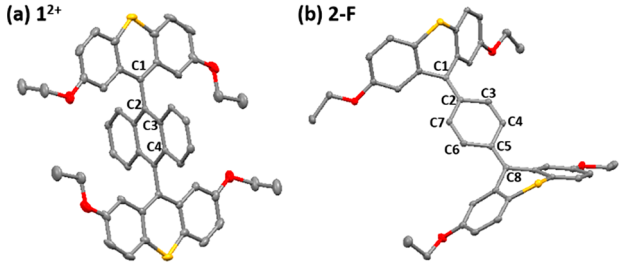

Figure 2. ORTEP drawings of the (a) 1^{2+} and (b) **2-F** structures. Hydrogen atoms, counterions, and solvent molecules are omitted for clarity.

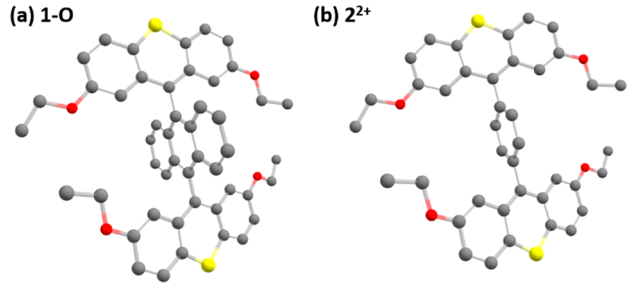

Figure 3. DFT-optimized structures of the (a) **1-O** and (b) 2^{2+} structures. Hydrogen atoms are omitted for clarity.

Figure 3b) adopt an almost orthogonal conformation of the aromatic spacers relative to the thioxanthylium units with dihedral angles of 80° and 75°, respectively. In both structures the two thioxanthylium motifs are coplanar. For 1^{2+}, the C1−C2 and C2−C3 distances are 1.494(3) and 1.407(3) Å, respectively, which shows that it does not have a quinoidal structure. DFT calculations predict a similar quasi orthogonal conformation for **1-O** similar to the dications with a dihedral angle of 82° between the anthracene spacer relative to the thioxanthenes (Figure 3a). In contrast, **2-F** has a double-folded boat-like structure (Figure 2b). Within one thiaxanthylidene the fold angle between the two C_6H_3OEt rings is 133°. The bond length of ∼1.38 Å between C5−C8 and C1−C2 and ∼1.35 Å between C6−C7 and C3−C4 are consistent with double-bond character. On the other hand, single-bond character was noted between C2−C7, C2−C3, C4−C5, and C5−C6 (∼1.45 Å). This reveals that **2-F** has a quinoidal closed-shell structure in the solid state.

Electronic Absorption and Emission Spectroscopy. The redox couple 1^{2+} and **1-O** both display UV/vis absorption spectra (Figure 4a and c, Table 1) with absorptions at long wavelength in the visible region between 500 and 650 nm. These are common bands for twisted geometries.[12,18,37−39] Thus, it seems likely that the conformation does not change significantly between 1^{2+} and **1-O**. The absorption bands for

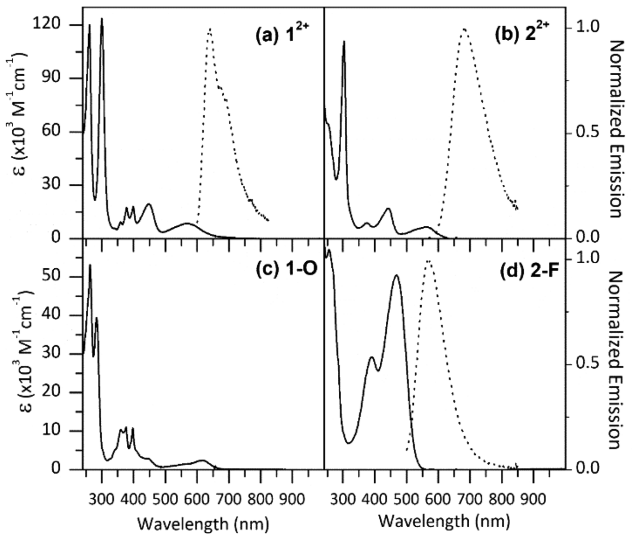

Figure 4. UV/vis absorption and normalized emission spectra (dotted lines) of (a) 1^{2+} (6.25×10^{-6} M), (b) 2^{2+} (6.25×10^{-6} M), (c) **1-O** (2.5×10^{-5} M), and (d) **2-F** (1.25×10^{-5} M) in DCM. Excitation wavelengths: (a) 560 nm, (b) 520 nm, and (d) 450 nm.

https://doi.org/10.1021/jacs.1c05938
J. Am. Chem. Soc. 2021, 143, 18020−18028

Table 1. λ_{max} Values for 1^{2+}, 2^{2+}, 1-O, and 2-F

	λ_{max} (nm)	
	UV/vis	emission (Φ^b)
(a) 1^{2+}	260, 299, 359, 377, 398, 448, 569	641 (0.02)
(b) 2^{2+}	253 (S[a]), 303, 376, 443, 561	682 (4.0)
(c) 1-O	264, 284, 340 (S), 360, 376, 397, 444, 614	
(d) 2-F	255, 391, 468	569

[a]S = shoulder. [b]Φ = quantum yield in %.

1^{2+} and 1-O between 325 and 400 nm with vibronic splitting are typical for anthracene.[33] In contrast, the spectra of 2^{2+} and 2-F (Figure 4b and d, Table 1) are consistent with a major change in geometry. 2-F shows a broad absorption band between 350 and 550 nm. The absorption bands at shorter wavelength are typical of an increase in S0−S1 gap expected for a folded structure. Its spectrum is similar to that observed for the folded anthracene-bridged bis-DMA, confirming its folded structure in solution,[18] while 2^{2+} shows characteristic absorptions of a twisted conformation.[12] Compound 1^{2+} exhibits red emission (λ_{max} = 641 nm), whereas 1-O is not luminescent as expected due to its triplet diradical character (*vide infra*). Furthermore, emission spectroscopy shows that reduction of 2^{2+} to 2-F results in a change in luminescence with λ_{max} shifting from 682 nm (red) to 569 nm (yellow), respectively.

EPR Spectroscopy. 1-O shows a typical EPR spectrum for a triplet diradical in toluene at 77 K (Figure 5). Simulation (EasySpin, see the SI) yields a *g*-value of 2.0023 and zero field splitting parameters D = 183 MHz (65.3 G) and E = 3 MHz. D was used to estimate a spin−spin distance of 7.53 Å by the point-dipole approximation.[26] This distance is greater than the distance between the two carbons at the 9-position (5.87 Å), which indicates delocalization of the unpaired electrons.[26,40] The forbidden Δm_s = 2 signal is observed at 1722 G (effective *g*-value of 4.006), the intensity of which increases with decreasing temperature. The Δm_s = 2 double integrated intensity (I_{EPR}) vs $1/T$ (temperature range 70−8.6 K) plot was fitted with the Bleaney−Bowers equation (eq 1), where C is the Curie constant, J is the electron exchange interaction, $2J$ equals $\Delta E_{S\text{-}T}$ (=+22 × 10^{-3} kcal mol^{-1}), and J = +3.9 cm^{-1} (ferromagnetic coupling).

$$I_{EPR} = \frac{C}{T}\frac{3e^{-2J/k_BT}}{1 + 3e^{-2J/k_BT}} \quad (1)$$

From both the paramagnetic ^{1}H NMR and EPR spectral data we conclude that 1-O has a triplet diradical ground state with a singlet diradical state slightly higher in energy. As expected, for compound 2-F a signal was not observed, consistent with its preferred closed-shell, folded (F) quinoidal structure (*vide supra*).

Computational Studies. DFT calculations on 1 and 2 were performed to further investigate the stabilities of the folded quinoidal geometries relative to the orthogonal diradical conformations. Computational investigation at the B3LYP/6-31** level of theory (for the selection of the computational method, see the SI) of the various possible geometries showed that the most stable geometry is a folded (F) structure for the neutral compounds 1 and 2 and an orthogonal (O) conformation for the dicationic compounds 1^{2+} and 2^{2+} (Tables S4, S5). More specifically, the most stable geometry of 1-F is in a doubly *anti*-folded state that minimizes steric

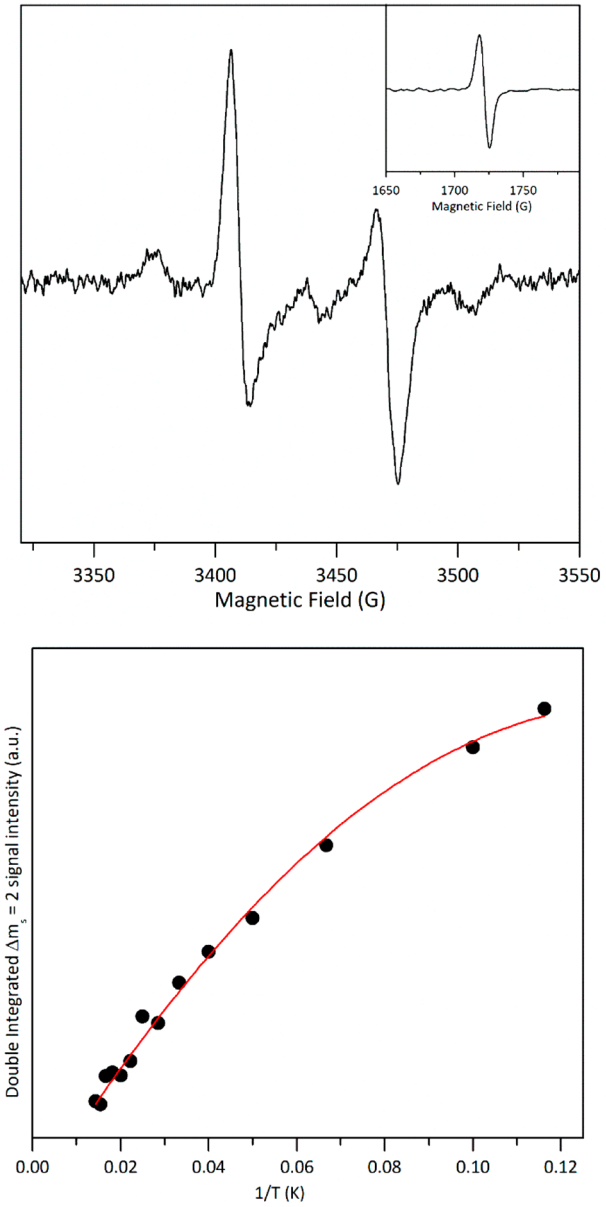

Figure 5. Top: EPR signal of compound 1-O (4.4 × 10^{-4} M) in toluene at 77 K with inset: forbidden Δm_s = 2 signal at 40 K. Bottom: Curie plot of 1-O with fit to the Bleaney−Bowers equation (adj. *R*-square = 0.9939).

hindrance with the anthracenyl bridge. For 2-F the steric hindrance is significantly lower, and it has a *syn*-folded orientation as its most stable form. However, the isomerization barriers of the neutral compounds differ greatly. Reduction of 1^{2+} leads to the diradical state 1-O without significant conformational change. 1-O is a local minimum (ΔE = 0.7 kcal mol^{-1} relative to 1-F, Figure 6) kinetically trapped with a high barrier ($\Delta E^{\ddagger}$ = 30.6 kcal mol^{-1}) for isomerization at room temperature toward the global minimum 1-F. Conversely, as deduced from electrochemistry (*vide infra*), the reduction of 2^{2+} does initially lead to 2-O, which subsequently isomerizes to 2-F. The calculated barrier for the latter process ($\Delta E^{\ddagger}$ = 9.5 kcal mol^{-1}) supports the experimental observations. The low barrier and relative energy differences between 2-O and 2-F provide a rationale for the shape of the cyclic voltammogram (Figure 7e), where a relatively fast equilibrium means that both

https://doi.org/10.1021/jacs.1c05938
J. Am. Chem. Soc. 2021, 143, 18020−18028

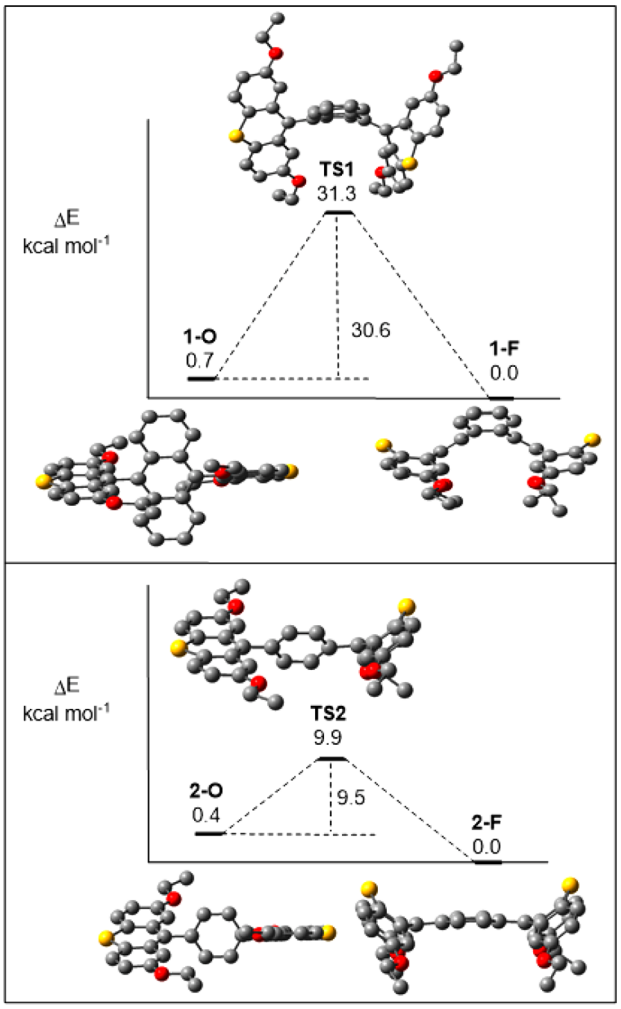

Figure 6. Schematic and graphic representation of the thermal isomerization pathway for the neutral geometries **1-O** to **1-F** and **2-O** to **2-F** based on DFT calculations (B3LYP/6-31G**). Hydrogens are omitted for clarity.

the orthogonal and folded structures are present in solution. This isomerization pathway was probed with a potential energy surface scan (Figures S22 and S23). The relative energies of the diradical singlets and the corresponding triplets for **1-O** and **2-O** are sufficiently close for population of both states ($\Delta E_{S\text{-}T} = -14 \times 10^{-3}$ kcal mol^{-1} for **1-O** and $\Delta E_{S\text{-}T} = -0.145$ kcal mol^{-1} for **2-O**). The low $\Delta E_{S\text{-}T}$ for **1-O** is in accordance with EPR data, although experimentally a triplet ground state was observed. However, the calculated energy difference is less than the expected error margin, and hence it can only be concluded that the energy levels are highly similar. For all diradical species we found that the spin density is mainly located on the thioxanthene motifs with negligible contribution from the bridging motifs.

Electrochemistry. Compounds $\mathbf{1}^{2+}$ and $\mathbf{2}^{2+}$ were characterized electrochemically by cyclic voltammetry in dichloromethane (DCM) at rt, and both show reversible electrochemical switching (Figure 7a and b, Table 2). For $\mathbf{1}^{2+}$ splitting of the redox waves was seen in DCM, whereas in MeCN (Figure S9) a single reversible wave was observed. This difference is due to the better solvation of the radical cation in MeCN after the first reduction relative to DCM.[41] In solvents with poor donor properties, such as DCM, the singly occupied

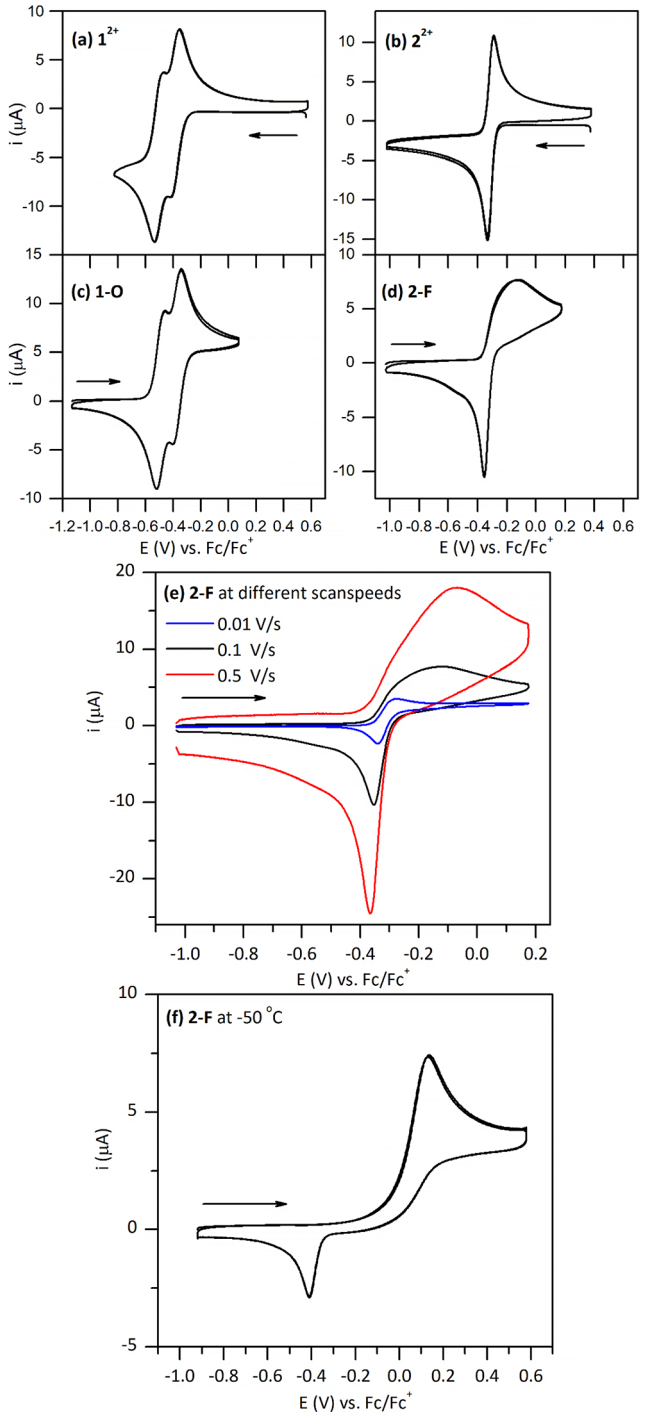

Figure 7. Cyclic voltammograms of (a) $\mathbf{1}^{2+}$, (b) $\mathbf{2}^{2+}$, (c) **1-O**, (d) **2-F** (0.1 V s^{-1}), (e) **2-F** at different scan rates, and (f) **2-F** at −50 °C (0.1 V s^{-1}) recorded in DCM with 5×10^{-4} M analyte and 0.1 M $TBAPF_6$.

Table 2. Peak- and Half-Wave Potentials for $\mathbf{1}^{2+}$, $\mathbf{2}^{2+}$, 1-O, and 2-F

	$E_{p,ox}$	$E_{p,red}$	$E_{1/2}$
(a) $\mathbf{1}^{2+}$	−0.47/−0.36	−0.42/−0.54	−0.39/−0.50
(b) $\mathbf{2}^{2+}$	−0.29	−0.33	−0.31
(c) **1-O**	−0.46/−0.34	−0.40/−0.52	−0.49/−0.37
(d) **2-F**	−0.12	−0.35	−0.24
(e) **2-F** (−50 °C)	0.14	−0.41	

https://doi.org/10.1021/jacs.1c05938
J. Am. Chem. Soc. 2021, 143, 18020−18028

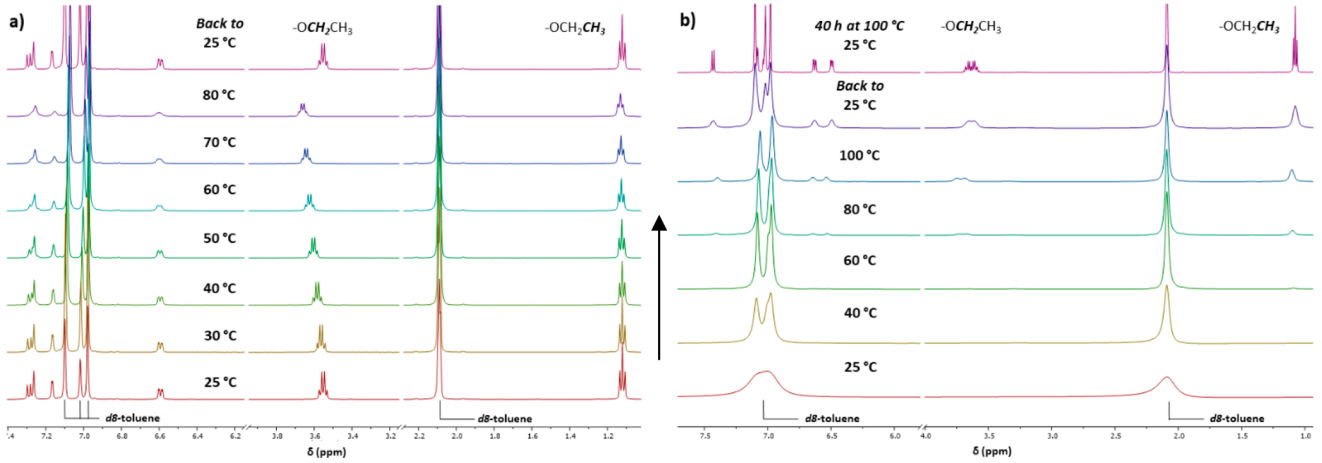

Figure 8. VT-NMR (500 MHz) spectroscopy studies of compounds (a) **2-F** and (b) **1-O** in toluene-d_8.

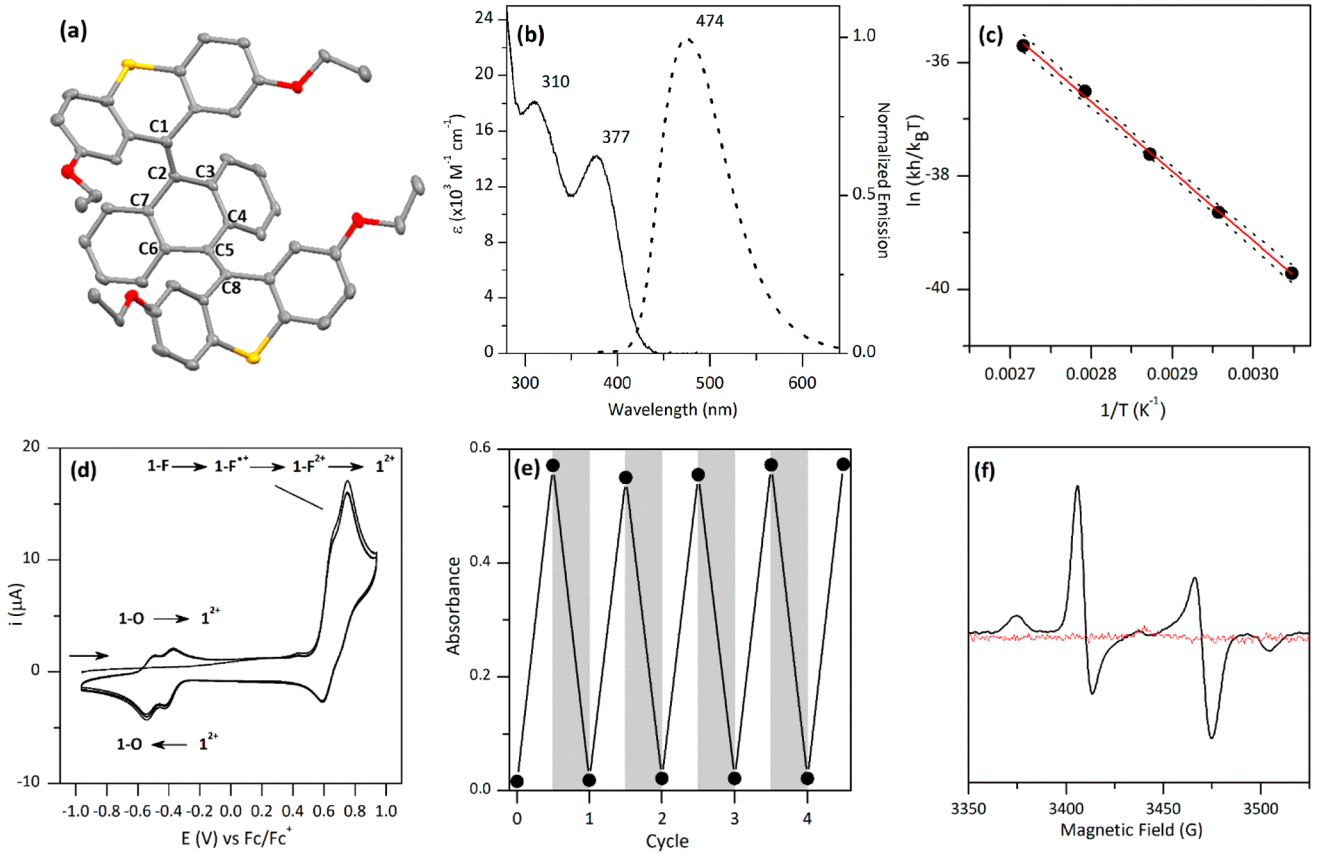

Figure 9. (a) ORTEP drawing of the **1-F** structure (hydrogen atoms are omitted for clarity), (b) UV/vis absorption and normalized emission spectrum (λ_{exc} = 350 nm) of **1-F** (2.5×10^{-5} M) in DCM including λ_{max} values (quantum yield = 6.9%), (c) Eyring–Polanyi plot of the thermal conversion of **1-O** to **1-F** in toluene monitored at 615 nm obtained by fitting to the linearized form of the Eyring equation (adj. *R*-square = 0.9985). Dashed lines indicate 95% confidence intervals, (d) cyclic voltammogram of **1-F**, $E_{p,ox1}$ = 0.66 V (shoulder) and $E_{p,ox2}$ = 0.75 V (5×10^{-4} M in DCM/0.1 M $TBAPF_6$/0.1 V s^{-1}), (e) cycles of irradiating (1×10^{-3} M) with 385 nm for 10 min (white areas) and heating at 90 °C for 1 h (gray areas) while monitoring the absorbance at 615 nm, and (f) EPR spectra of **1-F** (5.3×10^{-4} M) in toluene at 77 K: before irradiation (red) and after irradiation with 385 nm at rt for 10 min (black).

molecular orbital (SOMO) can be delocalized over the entire molecule, stabilizing the radical cation.[42] Therefore, in DCM, the second reduction of $\mathbf{1}^{2+}$ is shifted to more negative potentials. The radical cation of $\mathbf{2}^{2+}$ is less stabilized, and only a single reversible wave is observed independent of solvent. Cyclic voltammograms of **1-O** and **2-F** do not show hysteresis (Figure 7c and d, Table 2). This suggests that **1-O** has a structure similar to $\mathbf{1}^{2+}$. The open-shell diradical **1-O** indeed has an almost orthogonal conformation. In contrast, it is proposed that the folded closed-shell **2-F** is in equilibrium with the orthogonal open-shell diradical **2-O**. This explains why **2-F** exhibits a quasi-reversible cyclic voltammogram where the rapid prior equilibrium between **2-F** and **2-O** precedes the oxidation of **2-O** to $\mathbf{2}^{2+}$.[31,43,44] Hysteresis is not observed, as **2-**

https://doi.org/10.1021/jacs.1c05938
J. Am. Chem. Soc. 2021, 143, 18020−18028

O and $\mathbf{2}^{2+}$ have similar conformations. At lower scan rate there is more time (within the time frame of the electrochemical experiment) for the equilibrium to shift toward **2-O**, and the voltammogram shows increasing electrochemical reversibility (Figure 7e). Cyclic voltammetry at −50 °C shows the direct oxidation of **2-F** to $\mathbf{2}^{2+}$ (Figure 7f, Table 2). At this temperature the **2-O** state is not populated, and the large geometrical change from the folded **2-F** to the orthogonal $\mathbf{2}^{2+}$ is responsible for the hysteresis.

Thermal Equilibrium between 2-F and 2-O. Density functional theory (DFT) calculations indicated that the orthogonal diradical **2-O** is thermally accessible. Variable-temperature NMR (VT-NMR) spectroscopy studies of **2-F** (Figure 8a) show that the resolved signals at 25 °C become increasingly broadened with heating to 80 °C, consistent with the population of the excited triplet diradical state (**2-O**). Returning to 25 °C recovers the original spectrum as expected from the low activation barrier for the **2-O** to **2-F** conversion. These results are consistent with our electrochemical data and show that there is a thermal equilibrium between **2-F** and **2-O**.

Switching between 1-O and 1-F. DFT calculations predict that **1-F** is more stable than **1-O**, but it was not observed after the chemical reduction of $\mathbf{1}^{2+}$. We speculated that the as-synthesized **1-O** was kinetically trapped. VT-NMR studies on the paramagnetic compound **1-O** (Figure 8b) showed resolved signals, which are assigned to **1-F**, that emerged as the temperature was increased to 100 °C. Cooling to 25 °C shows that the signals persist, consistent with a high activation barrier for interconversion between **1-F** and **1-O**. Full conversion to **1-F** was achieved by holding the solution at 100 °C until its ^{1}H NMR spectrum at rt shows highly resolved signals. **1-O** was converted in toluene at 90 °C to isolate and characterize **1-F**. Single crystals of **1-F** were grown and confirmed a double *anti*-folded geometry (Figure 9a). Within one thiaxanthylidene the fold angle between the two C_6H_3OEt rings is 129°. A quinoidal structure was confirmed by the double-bond character of the C5−C8 and C1−C2 bonds (∼1.35 Å) and the single-bond character of the C4−C5, C5−C6, C2−C7, and C2−C3 bonds (∼1.50 Å). Its UV/vis absorption spectrum supports the hypothesis that a geometrical change from orthogonal to folded occurred as the longest wavelength absorption is shifted to 450 nm (Figure 9b). The emission spectrum of **1-F** has a maximum at 474 nm. Thus, by reversible switching between the $\mathbf{1}^{2+}$, **1-O**, and **1-F** states (*vide infra*) the luminescence can be changed between red, nonluminescent, and blue, respectively. The activation barrier for the **1-O** to **1-F** transition was determined by UV/vis absorption spectroscopy in toluene. The decay in absorbance was monoexponential, and rates were used in an Eyring−Polanyi plot (Figure 9c). Eyring−Polanyi analysis yielded the free energy of activation $\Delta G^{\ddagger}(293\ \mathrm{K}) = 25.7 \pm 0.2$ kcal mol^{-1}. The activation barrier from **1-O** to **1-F** rationalizes why the reduction of $\mathbf{1}^{2+}$ leads to trapping in the **1-O** state, as can be seen from the cyclic voltammograms of the $\mathbf{1}^{2+}$/**1-O** couple. The barriers are related to the increased steric hindrance in the fjord region, and this behavior is not seen for the **2O**/**2F** couple. This restricted movement in the fjord region is also reflected in the onset of the oxidation potential of **1-F** at 0.5 V (relative to the onset of the oxidation potential of **1-O** at −0.6 V) (Figure 9d). The lack of chemical reversibility for the oxidation of **1-F** is the result of the fast (within the time frame of the electrochemical experiment) chemical step $\mathbf{1\text{-}F}^{2+} \rightarrow \mathbf{1}^{2+}$. This chemical step leads to the observation of the following small reduction waves: $\mathbf{1\text{-}F}^{2+} \rightarrow \mathbf{1\text{-}F}^{+\bullet}$ followed by $\mathbf{1\text{-}F}^{+\bullet} \rightarrow$ **1-F** at peak potentials 0.7 V (shoulder) and 0.6 V, respectively. Oxidation of **1-F** (or **1-O**) leads to $\mathbf{1}^{2+}$, which can subsequently be reduced at −0.39 and −0.50 V to **1-O** in the return sweep (from 1 to −1 V). This hysteresis in the cyclic voltammogram is caused by a geometrical change.[18,45] Irradiation at 385 nm leads to photochemical switching from **1-F** to **1-O** (Figure 9e). In toluene a band at 615 nm assigned to **1-O** is observed. Heating at 90 °C results in this absorption band disappearing over 1 h. Repeated cycles of irradiation and heating confirm the excellent reversibility of this process not showing fatigue. Additional evidence for the photochemical back reaction of **1-F** to **1-O** was provided by EPR spectroscopy. Irradiation at 385 nm of the EPR-silent **1-F** leads to the emergence of signals associated with **1-O** (Figure 9f).

CONCLUSION

Here we report two arene-extended bis-thiaxanthylidines in which the introduction of an anthracene spacer allowed for redox switching between an orthogonal dicationic ($\mathbf{1}^{2+}$) and a diradical state (**1-O**), while thermal and photochemical switching allows modulation between **1-O** and the folded state **1-F**. The barrier between the neutral orthogonal open-shell triplet (**1-O**) and the folded closed-shell (**1-F**) form is high ($\Delta G^{\ddagger}(293\ \mathrm{K}) = 25.7$ kcal mol^{-1}), showing that **1-O** is a remarkably stable diradical. The reverse reaction from the closed-shell to the open-shell form has a higher activation barrier ($\Delta G^{\ddagger} = 31.3$ kcal mol^{-1} (from DFT)). The resultant three stable states of this system show that the reduction of $\mathbf{1}^{2+}$ leads to the kinetically trapped **1-O**, which can be switched thermally to the more stable folded geometry **1-F**. Irradiation of **1-F** switches it back to the open-shell **1-O**, while oxidation produces $\mathbf{1}^{2+}$. For the benzene analogue, redox switching between an orthogonal dicationic ($\mathbf{2}^{2+}$) and a diradical state (**2-O**) was observed. A thermal equilibrium was found between the neutral more stable folded closed-shell (**2-F**) and orthogonal open-shell (**2-O**) forms with a low activation barrier from the transient **2-O** to **2-F**. At low temperature **2-F** can be directly oxidized to $\mathbf{2}^{2+}$. We ascribe the difference in activation barrier between **2-O** to **2-F** *relative to* **1-O** to **1-F** to the increased steric bulk in the fjord region. Overall, this means a robust three-state switch has been developed where the dication $\mathbf{1}^{2+}$, diradical **1-O**, and **1-F** states can be individually addressed and interconverted by electricity, temperature control, or irradiation. This opens opportunities for the exploration of stable multistate photo- and electrochemical-responsive materials and devices.

ASSOCIATED CONTENT

Supporting Information

The Supporting Information is available free of charge at https://pubs.acs.org/doi/10.1021/jacs.1c05938.

Crystallographic data (ZIP)

Experimental procedures, crystallography, computational details, and full characterization of all new compounds (PDF)

Accession Codes

CCDC 2087865−2087867 contain the supplementary crystallographic data for this paper. These data can be obtained free of charge via www.ccdc.cam.ac.uk/data_request/cif, or by emailing data_request@ccdc.cam.ac.uk, or by contacting The

https://doi.org/10.1021/jacs.1c05938
J. Am. Chem. Soc. 2021, 143, 18020−18028

Cambridge Crystallographic Data Centre, 12 Union Road, Cambridge CB2 1EZ, UK; fax: +44 1223 336033.

AUTHOR INFORMATION

Corresponding Author

Ben L. Feringa − *Stratingh Institute for Chemistry and Zernike Institute for Advanced Materials, University of Groningen, 9747 AG Groningen, The Netherlands;* orcid.org/0000-0003-0588-8435; Email: b.l.feringa@rug.nl

Authors

Marco B. S. Wonink − *Stratingh Institute for Chemistry and Zernike Institute for Advanced Materials, University of Groningen, 9747 AG Groningen, The Netherlands*

Brian P. Corbet − *Stratingh Institute for Chemistry and Zernike Institute for Advanced Materials, University of Groningen, 9747 AG Groningen, The Netherlands*

Artem A. Kulago − *Stratingh Institute for Chemistry and Zernike Institute for Advanced Materials, University of Groningen, 9747 AG Groningen, The Netherlands*

Gregory B. Boursalian − *Stratingh Institute for Chemistry and Zernike Institute for Advanced Materials, University of Groningen, 9747 AG Groningen, The Netherlands*

Bas de Bruin − *Van't Hoff Institute for Molecular Sciences (HIMS), University of Amsterdam, 1098 XH Amsterdam, The Netherlands;* orcid.org/0000-0002-3482-7669

Edwin Otten − *Stratingh Institute for Chemistry and Zernike Institute for Advanced Materials, University of Groningen, 9747 AG Groningen, The Netherlands;* orcid.org/0000-0002-5905-5108

Wesley R. Browne − *Stratingh Institute for Chemistry and Zernike Institute for Advanced Materials, University of Groningen, 9747 AG Groningen, The Netherlands;* orcid.org/0000-0001-5063-6961

Complete contact information is available at: https://pubs.acs.org/10.1021/jacs.1c05938

Author Contributions

The manuscript was written through contributions of all authors. All authors have given approval to the final version of the manuscript.

Funding

This work was supported financially by the European Research Council (ERC; advanced grant no. 694345 to B.L.F.) and the Dutch Ministry of Education, Culture and Science (Gravitation program no. 024.001.035).

Notes

The authors declare no competing financial interest.

ACKNOWLEDGMENTS

We would like to thank the Center for Information Technology of the University of Groningen for their support and for providing access to the Peregrine high-performance computing cluster. We would like to thank Stefano Crespi for comments and suggestions regarding the computational studies. Jelte S. Steen is acknowledged for assistance with spectroelectrochemical measurements. Renze Sneep is acknowledged for mass spectral analysis.

REFERENCES

(1) van Leeuwen, T.; Lubbe, A. S.; Štacko, P.; Wezenberg, S. J.; Feringa, B. L. Dynamic Control of Function by Light-Driven Molecular Motors. *Nat. Rev. Chem.* **2017**, *1*, 0096.

(2) Dattler, D.; Fuks, G.; Heiser, J.; Moulin, E.; Perrot, A.; Yao, X.; Giuseppone, N. Design of Collective Motions from Synthetic Molecular Switches, Rotors, and Motors. *Chem. Rev.* **2020**, *120*, 310−433.

(3) Krause, S.; Feringa, B. L. Towards Artificial Molecular Factories from Framework-Embedded Molecular Machines. *Nat. Rev. Chem.* **2020**, *4*, 550−562.

(4) Russew, M. M.; Hecht, S. Photoswitches: From Molecules to Materials. *Adv. Mater.* **2010**, *22*, 3348−3360.

(5) Coskun, A.; Spruell, J. M.; Barin, G.; Dichtel, W. R.; Flood, A. H.; Botros, Y. Y.; Stoddart, J. F. High Hopes: Can Molecular Electronics Realise Its Potential? *Chem. Soc. Rev.* **2012**, *41*, 4827−4859.

(6) Szymański, W.; Beierle, J. M.; Kistemaker, H. A. V.; Velema, W. A.; Feringa, B. L. Reversible Photocontrol of Biological Systems by the Incorporation of Molecular Photoswitches. *Chem. Rev.* **2013**, *113*, 6114−6178.

(7) Baroncini, M.; Silvi, S.; Credi, A. Photo- And Redox-Driven Artificial Molecular Motors. *Chem. Rev.* **2020**, *120*, 200−268.

(8) Feringa, B. L.; Browne, W. R. *Molecular Switches*; Wiley-VCH: Weinheim, Germany, 2011.

(9) Feringa, B. L.; van Delden, R. A.; Koumura, N.; Geertsema, E. M. Chiroptical Molecular Switches. *Chem. Rev.* **2000**, *100*, 1789−1816.

(10) Kida, N.; Hikita, M.; Kashima, I.; Okubo, M.; Itoi, M.; Enomoto, M.; Kato, K.; Takata, M.; Kojima, N. Control of Charge Transfer Phase Transition and Ferromagnetism by Photoisomerization of Spiropyran for an Organic-Inorganic Hybrid System, $(SP)[Fe^{II}Fe^{III}(dto)_3]$ (SP = spiropyran, dto = $C_2O_2S_2$). *J. Am. Chem. Soc.* **2009**, *131*, 212−220.

(11) Ishigaki, Y.; Harimoto, T.; Sugawara, K.; Suzuki, T. Hysteretic Three-State Redox Interconversion among Zigzag Bisquinodimethanes with Non-Fused Benzene Rings and Twisted Tetra-/Dications with [5]/[3]Acenes Exhibiting Near-Infrared Absorptions. *J. Am. Chem. Soc.* **2021**, *143*, 3306−3311.

(12) Browne, W. R.; Pollard, M. M.; De Lange, B.; Meetsma, A.; Feringa, B. L. Reversible Three-State Switching of Luminescence: A New Twist to Electro- and Photochromic Behavior. *J. Am. Chem. Soc.* **2006**, *128*, 12412−12413.

(13) Ragazzon, G.; Baroncini, M.; Silvi, S.; Venturi, M.; Credi, A. Light-Powered Autonomous and Directional Molecular Motion of a Dissipative Self-Assembling System. *Nat. Nanotechnol.* **2015**, *10*, 70−75.

(14) Xu, F.; Pfeifer, L.; Crespi, S.; Leung, F. K.-C.; Stuart, M. C. A.; Wezenberg, S. J.; Feringa, B. L. From Photoinduced Supramolecular Polymerization to Responsive Organogels. *J. Am. Chem. Soc.* **2021**, *143*, 5990−5997.

(15) Dorel, R.; Feringa, B. L. Photoswitchable Catalysis Based on the Isomerisation of Double Bonds. *Chem. Commun.* **2019**, *55*, 6477−6486.

(16) Zhang, Y.; Zheng, Y.; Zhou, H.; Miao, M.-S.; Wudl, F.; Nguyen, T.-Q. Temperature Tunable Self-Doping in Stable Diradicaloid Thin-Film Devices. *Adv. Mater.* **2015**, *27*, 7412−7419.

(17) Kurata, H.; Tanaka, T.; Oda, M. Dibenzoannulated 3,5,3″,5″-Tetra(*t*-butyl)-*p*-terphenoquinone. A Reversible, Photochemical-Thermal Switching System Involving Restricted Conformational Change. *Chem. Lett.* **1999**, *28*, 749−750.

(18) Nishiuchi, T.; Ito, R.; Stratmann, E.; Kubo, T. Switchable Conformational Isomerization of an Overcrowded Tristricyclic Aromatic Ene. *J. Org. Chem.* **2020**, *85*, 179−186.

(19) Sakamaki, D.; Ito, A.; Tsutsui, Y.; Seki, S. Tetraaza[1_4]- and Octaaza[1_8]paracyclophane: Synthesis and Characterization of Their Neutral and Cationic States. *J. Org. Chem.* **2017**, *82*, 13348−13358.

(20) Ni, Y.; Gopalakrishna, T. Y.; Wu, S.; Wu, J. A Stable All-Thiophene-Based Core-Modified [38]Octaphyrin Diradicaloid: Con-

formation and Aromaticity Switch at Different Oxidation States. *Angew. Chem., Int. Ed.* **2020**, *59*, 7414−7418.
(21) Hu, X.; Wang, W.; Wang, D.; Zheng, Y. The Electronic Applications of Stable Diradicaloids: Present and Future. *J. Mater. Chem. C* **2018**, *6*, 11232−11242.
(22) Biedermann, P. U.; Stezowski, J. J.; Agranat, I. Conformational Space and Dynamic Stereochemistry of Overcrowded Homomerous Bistricyclic Aromatic Enes − A Theoretical Study. *Eur. J. Org. Chem.* **2001**, *2001*, 15−34.
(23) Kassem, S.; van Leeuwen, T.; Lubbe, A. S.; Wilson, M. R.; Feringa, B. L.; Leigh, D. A. Artificial Molecular Motors. *Chem. Soc. Rev.* **2017**, *46*, 2592−2621.
(24) Tschitschibabin, A. E. Über einige Phenylierte Derivate des p,p-Ditolyls. *Ber. Dtsch. Chem. Ges.* **1907**, *40*, 1810−1819.
(25) Montgomery, L. K.; Huffman, J. C.; Jurczak, E. A.; Grendze, M. P. The Molecular Structures of Thiele's and Chichibabin's Hydrocarbons. *J. Am. Chem. Soc.* **1986**, *108*, 6004−6011.
(26) Abe, M. Diradicals. *Chem. Rev.* **2013**, *113*, 7011−7088.
(27) Kubo, T.; Shimizu, A.; Sakamoto, M.; Uruichi, M.; Yakushi, K.; Nakano, M.; Shiomi, D.; Sato, K.; Takui, T.; Morita, Y.; Nakasuji, K. Synthesis, Intermolecular Interaction, and Semiconductive Behavior of a Delocalized Singlet Biradical Hydrocarbon. *Angew. Chem., Int. Ed.* **2005**, *44*, 6564−6568.
(28) Porter, W. W.; Vaid, T. P.; Rheingold, A. L. Synthesis and Characterization of a Highly Reducing Neutral "Extended Viologen" and the Isostructural Hydrocarbon 4,4″″-Di-n-octyl-p- quaterphenyl. *J. Am. Chem. Soc.* **2005**, *127*, 16559−16566.
(29) Rudebusch, G. E.; Zafra, J. L.; Jorner, K.; Fukuda, K.; Marshall, J. L.; Arrechea-Marcos, I.; Espejo, G. L.; Ponce Ortiz, R.; Gómez-García, C. J.; Zakharov, L. N.; Nakano, M.; Ottosson, H.; Casado, J.; Haley, M. M. Diindeno-Fusion of an Anthracene as a Design Strategy for Stable Organic Biradicals. *Nat. Chem.* **2016**, *8*, 753−759.
(30) Yin, X.; Low, J. Z.; Fallon, K. J.; Paley, D. W.; Campos, L. M. The Butterfly Effect in Bisfluorenylidene-Based Dihydroacenes: Aggregation Induced Emission and Spin Switching. *Chem. Sci.* **2019**, *10*, 10733−10739.
(31) Ishigaki, Y.; Hashimoto, T.; Sugawara, K.; Suzuki, S.; Suzuki, T. Switching of Redox Properties Triggered by a Thermal Equilibrium between Closed-Shell Folded and Open-Shell Twisted Species. *Angew. Chem., Int. Ed.* **2020**, *59*, 6581−6584.
(32) Tang, B.; Zhao, J.; Xu, J. F.; Zhang, X. Tuning the Stability of Organic Radicals: From Covalent Approaches to Non-Covalent Approaches. *Chem. Sci.* **2020**, *11*, 1192−1204.
(33) Zeng, Z.; Sung, Y. M.; Bao, N.; Tan, D.; Lee, R.; Zafra, J. L.; Lee, B. S.; Ishida, M.; Ding, J.; López Navarrete, J. T.; Li, Y.; Zeng, W.; Kim, D.; Huang, K. W.; Webster, R. D.; Casado, J.; Wu, J. Stable Tetrabenzo-Chichibabin's Hydrocarbons: Tunable Ground State and Unusual Transition between Their Closed-Shell and Open-Shell Resonance Forms. *J. Am. Chem. Soc.* **2012**, *134*, 14513−14525.
(34) Balaban, A. T. Aromaticity of Six-Membered Rings with One Heteroatom. In *Topics in Heterocyclic Chemistry: Aromaticity in Heterocyclic Compounds*; Krygowski, T. M., Cyrański, M. K., Eds.; Springer: Berlin, Heidelberg, 2009; Vol. *19*, pp 204−246.
(35) Okada, K.; Imakura, T.; Oda, M.; Kajiwara, A.; Kamachi, M.; Yamaguchi, M. Remarkable Heteroatom Dependence of the Spin Multiplicity in the Ground State of 9,9′-(m-Phenylene)dixanthyl and -dithioxanthyl Diradicals. *J. Am. Chem. Soc.* **1997**, *119*, 5740−5741.
(36) Suzuki, T.; Nishida, J.-I.; Ohkita, M.; Tsuji, T. Preparation, Structure, and Redox Reactions of Nine-Membered Cyclic Peroxides: A Novel Electrochromic System Undergoing Reversible Extrusion and Trapping of O_2. *Angew. Chem., Int. Ed.* **2000**, *39*, 1804−1806.
(37) Matsuo, Y.; Wang, Y.; Ueno, H.; Nakagawa, T.; Okada, H. Mechanochromism, Twisted/Folded Structure Determination, and Derivatization of (*N*-Phenylfluorenylidene)acridane. *Angew. Chem., Int. Ed.* **2019**, *58*, 8762−8767.
(38) Hamamoto, Y.; Hirao, Y.; Kubo, T. Biradicaloid Behavior of a Twisted Double Bond. *J. Phys. Chem. Lett.* **2021**, *12*, 4729−4734.
(39) Ishigaki, Y.; Sugawara, K.; Yoshida, M.; Kato, M.; Suzuki, T. Two-Way Chromic Systems Based on Tetraarylanthraquinodimethanes: Electrochromism in Solution and Mechanofluorochromism in a Solid State. *Bull. Chem. Soc. Jpn.* **2019**, *92*, 1211−1217.
(40) Hirao, Y.; Konishi, A.; Kubo, T. Anthroxyl-Based Biradical: Toward the Construction of Highly Stable Multi-Spin Systems. *Org. Chem. Front.* **2017**, *4*, 828−833.
(41) Phelps, J.; Bard, A. J. One- vs. Two-Electron Oxidations of Tetraarylethylenes in Aprotic Solvents. *J. Electroanal. Chem. Interfacial Electrochem.* **1976**, *68*, 313−335.
(42) Browne, W. R.; De Jong, J. J. D.; Kudernac, T.; Walko, M.; Lucas, L. N.; Uchida, K.; van Esch, J. H.; Feringa, B. L. Oxidative Electrochemical Switching in Dithienylcyclopentenes, Part 1: Effect of Electronic Perturbation on the Efficiency and Direction of Molecular Switching. *Chem. - Eur. J.* **2005**, *11*, 6414−6429.
(43) Nelsen, S. F.; Echegoyen, L.; Evans, D. H. Electrochemical Detection of Conformational Equilibria in Tetraalkylhydrazines. *J. Am. Chem. Soc.* **1975**, *97*, 3530−3532.
(44) Nelsen, S. F.; Echegoyen, L.; Clennan, E. L.; Evans, D. H.; Corrigan, D. A. Low-Temperature Cyclic Voltammetry. 2. Conformational Analysis of Cyclic Tetraalkylhydrazines. *J. Am. Chem. Soc.* **1977**, *99*, 1130−1134.
(45) Olsen, B. A.; Evans, D. H. Electron-Transfer Reactions and Conformationl Changes Associated with the Reduction of Bianthrone. *J. Am. Chem. Soc.* **1981**, *103*, 839−843.

https://doi.org/10.1021/jacs.1c05938
J. Am. Chem. Soc. 2021, 143, 18020−18028